3

Carbon nanotube and graphene photonic devices: nonlinearity enhancement and novel preparation approaches

Y-W. SONG, Korea Institute of Science and Technology (KIST), South Korea

DOI: 10.1533/9780857098627.1.57

Abstract: With their nano-scaled dimensions and extremely elevated optical nonlinearity, carbon nanostructures including single-walled carbon nanotubes and graphene have played critical role in generating ultrafast optical pulses. The pulsation relies on passive mode-locking of the nanostructures, and has been enhanced by employing an evanescent field interaction scheme that guarantees the all-fiber high-power operation. Preparation schemes for pulsating devices have been evolving via the development of elegant processes such as optical deposition, electrospray, and aerosol deposition of carbon nanostructures, ensuring the dramatic increase of process efficiency. In this chapter, details of the technical achievements are addressed.

Key words: single-walled carbon nanotube, graphene, optical nonlinearity, saturable absorption, mode-locked laser.

3.1 Introduction

For decades, nanotechnology has been moving the paradigm of electronic devices by its unique contribution that cannot be cloned by conventional bulk technologies. The technical fusion with nanotechnology has also enabled new approaches that can solve the critical problems of conventional optical technology.

Mode-locked fiber lasers are a key source of sub-picosecond optical pulses to replace bulk solid-state lasers in many research/industrial fields that need high quality optical pulses within a very limited space and energy margin. Among typical mode-locking schemes, passive mode-locking (especially by using a saturable absorber) is attractive because of its structural simplicity and fast recovery operation, resulting in speedy loss modulation inside the cavity and much shorter pulses compared with active mode-locking.[1–4]

Optical nonlinearities of carbon nanostructures have been applied mainly to demonstrate high-speed laser technology controlled by passive

mode-locking of the lasers operated by nonlinear saturable absorption. Because of their (i) ultrafast recovery time; (ii) wide operating spectral window in telecommunications; (iii) high optical damage threshold; (iv) low threshold level of operation; (v) chemical stability; and (vi) a nano-footprint that is directly correlated with operational stability, the carbon nanostructures ensure the high performance of optical devices.[5, 6]

As a frontier nanomaterial, single-walled carbon nanotubes (SWNTs) have been researched intensively, notably contributing to the renovation of conventional optical devices that rely on semiconductor processes or bulk optics.[7–11] Unfortunately, they still have drawbacks, including (i) the agglomeration of individual nanostructures; (ii) difficult control of alignment and morphological factors, including chirality and diameter for energy bandgap design; and (iii) poor stability and long-term reliability because of their high surface energy. Recently, graphene, a 2-dimensional atomic layer that has advantages over the 1-dimensional carbon nanostructures including high operating speed and spectral availability as well as high process efficiency, has provided more opportunities to place both electronic and optical devices as substantiated enablers for future flexible devices.[12–14]

However, for the complete replacement of conventional components with nanostructure-based ones, limitations of the carbon nanostructures originating in nonlinear operation schemes and process efficiency need to be overcome. In this chapter, the principle of nonlinear saturable absorption and a novel light–nanostructure interaction scheme in forming ultrashort laser pulses are explained. In addition, elegant approaches toward high process efficiency to produce carbon nanostructure-based mode-locked lasers are reviewed.

3.2 Nonlinearity of carbon nanotubes and graphene; saturable absorption

Realization of all-fiber configurations of optic devices and systems has been a major research goal targeting because of their simple structure and efficient light control. In spite of the many advantages of fiber optics, nonlinearities that offer either a positive or negative effect on the required operation, and the operational stability that originates from the long length of the components should be considered as critical factors to be controlled. Stability can be improved by switching the long, unstable fiber section with the nanomaterials that can function in the minimized space while preserving the required nonlinearity.

3.2.1 Nonlinear saturable absorption in SWNTs and graphene

Carbon nanostructure technology has recently emerged as a key enabler for next-generation, passive mode-locking and noise suppression of lasers as

well as ultrafast optical switching.[5,15–18] SWNTs and graphene have a notable saturable absorption that creates mode-locked lasers in which photons with low intensity are absorbed but those with high intensity saturate the absorption and thereby pass through the absorber. The Dirac fermions excited by photon absorption lose energy by coupling with π-plasmons and 2D phonons (including distorted ones) in the carbon matrix, therefore the 'cooling down' satisfies the Fermi–Dirac distribution of the excited carriers in the energy band structure. As the number of photons increase, the generated carriers fill the energy states to a degree that more electron excitation is not allowed by the Pauli expulsion of occupying carriers at the edge of the filled energy band, thus the following photons with a specific wavelength can penetrate the nanostructures with no further absorption. In this manner, SWNTs can provide a 'synchronization point' to lock the phases of the propagating modes of the laser which induces passive pulsation.

The features of carbon nanostructures compared with conventional semiconductor components are summarized in Table 3.1. Normally, as can be seen in Fig. 3.1, the absorption bands of the carbon nanostructures cover a wide range of telecom windows. In case of SWNTs (see Fig. 3.1(a)), huge major absorption peak can be found as a result of the strong band edge-to-edge absorption in the semiconducting energy band structure. The absorption can be classified by two regimes, such as linear and nonlinear absorption. Linear absorption is directly proportional to the density of carbon atoms regardless of the isomeric evolution of the carbon nanostructures. On the other hand, nonlinear absorption depends on the crystal quality and morphology of the nanostructures. Figure 3.1(b) explains conceptually the nonlinear

Table 3.1 Summarized key properties of carbon nanostructures compared with conventional semiconductor-based devices

	Semiconductor-based devices	SWNT	Graphene
Recovery time	~1 ps	~500 fs	~200 fs
Operating spectrum	Narrow	Wide	Super wide
Nonlinear absorption	High	High (up to 10%)	Low (~3%)
Saturable absorption threshold	?	5.1 MW/cm^2	0.7 MW/cm^2
Optical damage threshold	Low	Middle (>500°C)	Middle
Nonlinear coefficient	?	$\gamma_{theory} = 10^8\,W^{-1}km^{-1}$	?
Fabrication	Complex, costly	Simpler	Simplest
Fiber compatibility	Good	Excellent	Excellent
Beam transmission	No	Yes	Yes
Optic/electric interfaces	?	Yes	Yes
Integration	Good	Excellent	Excellent

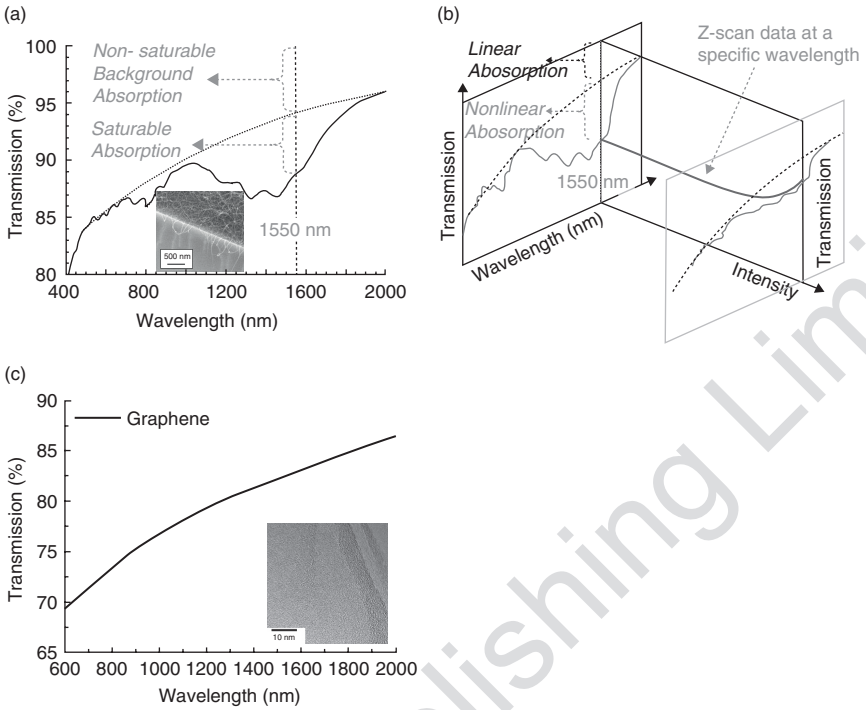

3.1 (a) Typical transmission characteristics of SWNTs, and (b) their evolution according to the light intensity. (c) Typical transmission characteristics of graphene. Insets represent the SEM image of the nanostructures.

absorption change as a function of light intensity at a fixed wavelength but the linear absorption is independent of the intensity. Experimentally, it has been shown that nonlinear absorption greater than 5% can facilitate passive mode-locking dramatically.

Recently, graphene has emerged as the replacement for SWNTs, providing a comparable nonlinear saturation effect.[19–22] In the case of graphene, a wider range of operation (>2.5 μm) can be guaranteed that originates from its point bandgap structures.[19, 23–26] It means that, unlike SWNTs, the operation wavelength of graphene for the saturable absorption is no longer limited by the energy bandgap. Typical transmission characteristics of graphene prepared by the modified Hummer method[27] are presented in Fig. 3.1(c). It has been reported that the intensity of the nonlinear absorption of graphene layers is inversely proportional to the number of the overlapped atomic layers.[20] Thus the dispersion and stabilization of the individual graphene flakes is the key to maximizing the saturable absorption effect. The transmittance for ideal 2-dimensional Dirac fermions in graphene is expressed as $T = (1 + 0.5\pi\alpha)^{-2}$,

where α is the fine structure constant that depicts the coupling of the propagating light with relativistic electrons. Taking into account graphene's nonlinearity and hydrocarbon contamination, the real transmittance shows that the graphene layer is less transparent at shorter wavelengths.[12,28] It is also thought that light scattering increases as the wavelength approaches the crystal coherence length, which contributes to the high absorption at shorter wavelengths.

3.2.2 Conventional SWNT mode-lockers and fiber pulsed lasers

Conventionally, SWNT mode lockers are fabricated by forming the SWNT layer on a transparent substrate, and then inserting it into the laser cavity. Either collimating by lenses or sandwiching between fiber ferrules can be used for the insertion of the device. Figures 3.2(a) and 3.2(b) describe the conventional mode lockers with the SWNT layers coated on a glass substrate and fiber ferrules, respectively. The prepared mode lockers are located within a fiber ring laser cavity, as shown in Fig. 3.2(c), which represents a typical structure of the passively pulsed laser. In the structure, a homogeneous gain medium, Er-doped fiber amplifier (EDFA), provides the intracavity gain. The isolator ensures unidirectional operation and suppression of sub-cavity formation. A polarization controller (PC) is used to

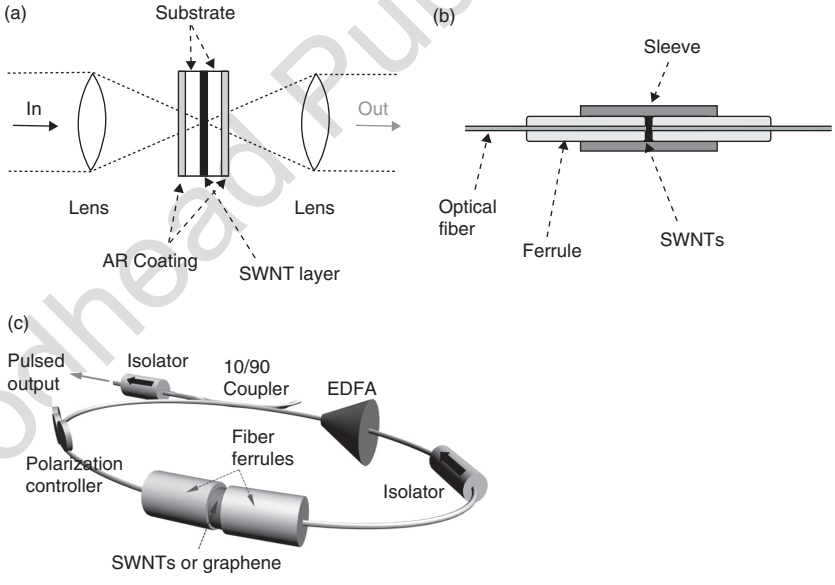

3.2 Conventional carbon nanostructure-based saturable absorbers of (a) free-space type, and (b) fiber ferrule type. (c) Typical setup of passively mode-locked fiber lasers.

match the round-trip polarization state in the fiber cavity. A part of the laser power is tapped using a fiber coupler yielding the laser output and the rest of the power is fed back into the cavity. The output coupling ratio can be controlled with ratio-diversified fiber couplers considering both intracavity power budget and output power. An additional piece of single-mode fiber (SMF) can be added to optimize the chromatic dispersion in the cavity so that the dispersion and nonlinearity can be balanced out to form the soliton-like short pulses by passive mode-locking.

3.3 Novel interaction schemes of propagating light with carbon nanostructures

In conventional SWNT and graphene fiber-optic devices in which the nanostructures are coated on to a flat substrate and located in the light path, despite the outstanding properties of the carbon nanostructures, functionality deteriorates because of the free space coupling, which causes the additional loss and deleterious reflection as well as an alignment problem. In the improved scheme, the fiber ferrule-type mode lockers serve widely to realize the passively mode-locked lasers with their excellent fiber compatibility along with the simple preparation process.[29] However, this scheme can cause distortion and/or damage to the nanostructures by physically touching the nanotubes. Also, the nonlinear absorption of the deposited nanostructure layer that is directly proportional to the material density of the layer is restricted by the background absorption (linear absorption) which also increases with the density. Most important, the carbon nanostructure-based mode lockers also suffer from optical power-induced thermal damage such that the nanostructures are burned out with optical power greater than 30 mW. Therefore, to guarantee the maximized efficiency of nonlinear effects from the carbon nanostructures, and to keep the mode lockers operating for more efficient and robust pulse formation in the high-energy operation that can provide inroads for diversified practical applications, it is necessary to develop a scheme to circumvent the damage to the carbon nanostructures, made of thermally fragile carbon network-based materials.

An evanescent field interaction scheme of propagating light with the nanostructures deposited on an all-fiber substrate was introduced, targeting the safe and robust operation of the carbon nanostructures while overcoming the optical power-induced thermal damage to them.[30] Compared with the direct interaction scheme (see Fig. 3.3(a)), the evanescent field interaction illustrated in Fig. 3.3(b) works in a non-blocking and material-safe way. When the effective refractive index of a part of the optical fiber is reduced, the propagating mode field is broadened, thereby enhancing the field's intensity (in this case, the evanescent field) at the fiber surface. When

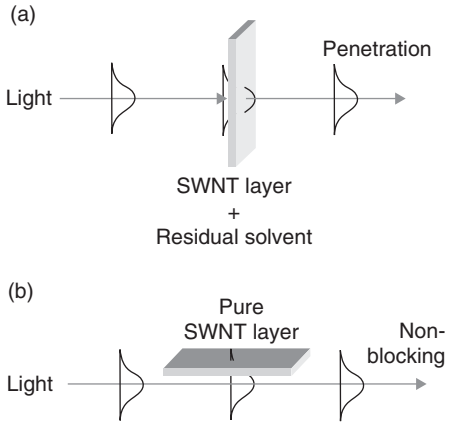

3.3 Interaction schemes of the propagating light and nanotubes layers: (a) direct interaction, and (b) evanescent field interaction.

the carbon nanostructures are placed on the surface, an intensified interaction of the evanescent field and the nanostructure can be expected. By side-polishing or tapering the optical fiber, thus replacing the silica with air, the index can be controlled. The advantages of this method includes (i) high power management by using a part of the mode's power to form equivalent ultrashort pulses in a non-blocking, all-fiber configuration; (ii) a long interaction length for the guided light and the nanostructures, which guarantees the efficient nonlinear effect, thereby facilitating the laser mode-locking in various nonoptimally conditioned laser cavities; (iii) an all-fiber non-blocking configuration; (iv) the individual nanostructures are not physically touched by other intracavity components; and (v) a possible application to ultrafast optical switches.

3.3.1 Single-walled carbon nanotube-deposited side-polished fibers as mode lockers

The propagating mode along the optical fiber has an evanescent field whose distribution is sensitive to the effective refractive index of the medium. The mode field can become broader with a low index. To achieve the low refractive index near the fiber core, side-polished fiber (i.e. D-shaped fiber) is prepared. After fixing a single-mode fiber (SMF) on to a holding block that has a V-groove to guide the SMF, epoxy is added to solidify the fiber-loaded block. The fiber is polished in four steps to make sure there is a smooth surface with no cracks, to minimize beam scattering through the polished surface. During the polishing process, the insertion loss that indicates the distance from the fiber core to the polished surface is checked and adjusted to about 3 dB.

SWNTs or graphene nanoflakes are deposited using an aerosol spray method. The nanostructures are dispersed in a solvent (usually dimethylformamide – DMF) that has strong dipoles. During spraying, the drying process is controlled to prevent the nanostructures either from being agglomerated along the surface of the solvent particles or being detached from the substrate because of rapid drying. The sample preparation is completed by protecting the deposited layers. The morphology of the nanostructures on the side-polished fiber should be preserved as they are deposited, to maintain their original absorption characteristics. The prepared device is shown in Fig. 3.4(a) with the schematic explanation of the operation (see Fig. 3.4(b)), where SWNTs are employed as the nonlinear materials.

By applying this device to the short-pulse formation in the laser structure illustrated in Fig. 3.2(c), passive mode-locking was demonstrated successfully, as shown in Fig. 3.5.[30] The demonstrated spectrum of the mode-locked laser has the center wavelength of 1556.2 nm (see Fig. 3.5(a)). The spectral half-width of 3.7 nm indicates the calculated pulse width of 685 fs when a transform-limited sech^2 pulse waveform is assumed. Figure 3.5(b) shows the second-harmonic generation (SHG) autocorrelation trace of our laser

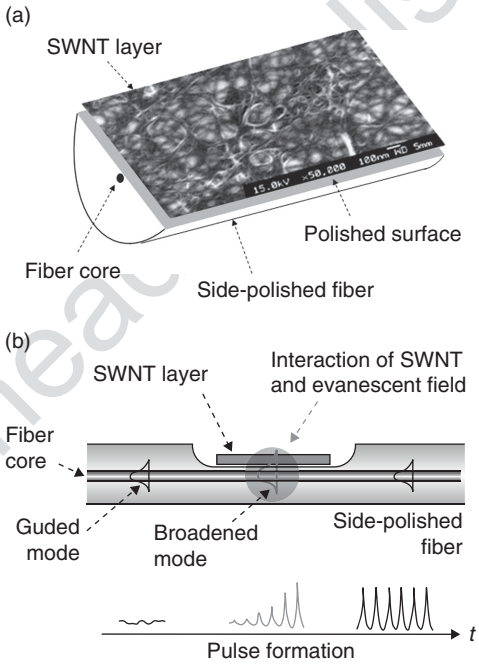

3.4 (a) Side-polished fiber coated with SWNTs on the flat polished surface, and (b) the explanation of the operation of the evanescent field interaction device with side-polished fiber.

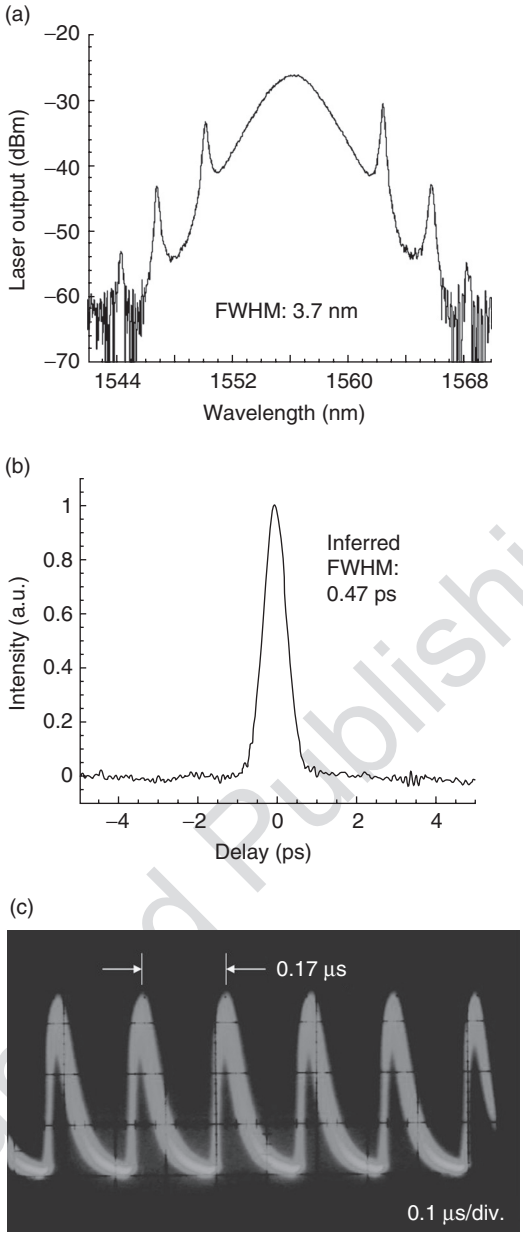

3.5 (a) Soliton-like optical spectrum of laser output pulsed by our mode locker showing the full-width half-maximum of 3.7 nm. (b) Autocorrelation trace of the mode-locked laser output measured with 50 fs resolution. (c) Output pulse train with the repetition rate of 5.88 MHz.

output measured with the resolution of 50 fs. Knowing the inferred pulse width of about 0.47 ps, it was found that the output pulses are somewhat remote from the transform-limited pulses, and that the pulses are more compressed by the additional fiber employed for guiding the output. The time-bandwidth product of the output is 0.216. Figure 3.5(c) represents the output pulse train measured by a high-speed photo-detector and an oscilloscope with a 0.1 ms/div time scale. It verifies the pulsed output and shows that the repetition rate is 5.88 MHz.

3.3.2 Aligned SWNTs on side-polished fibers

The interaction of light and SWNTs that has been limited by the randomized morphology of the nanostructures can be enhanced by their alignment, since only SWNTs whose direction is aligned with the light's electric field can ensure the saturable absorption effect. In Fig. 3.6, anisotropic absorption of an individual SWNT is described (Fig. 3.6(a))[31–33] and randomized (Fig. 3.6(b)), and aligned SWNTs (Fig. 3.6(c)) are compared in terms of polarized mode absorption.

A new scheme for the SWNT mode locker incorporating a vertically aligned single-walled carbon nanotube (VA-SWNT) film that can be attached to an arbitrary substrate using only hot water has been reported.[34] The thick film is prepared on a glass substrate (see Fig. 3.7(a)), limiting the degree of freedom for nanotube growth by controlling the density of the nucleation site. The lower surface of the film, which forms an interface with the glass substrate is hydrophobic, such that the film can be separated easily by water penetration (see Fig. 3.7(b)). For real sample fabrication, the film-coated substrate is immersed in hot water and the film is separated and floats on the water surface while the substrate sinks to the bottom. For the all-fiber configuration with improved operation efficiency and the preparation process, the VA-SWNT film is attached to a D-shaped fiber so that the evanescent field of guided light whose polarization is perpendicular to the film and parallel to the individual SWNTs has intensive and lengthy interaction with the nanotubes. This scheme has remarkable advantages, including (i) a simple and safe SWNT deposition process; (ii) maximized SWNT interaction with the field of propagating light because of the SWNT alignment, therefore also a low SWNT density threshold to achieve mode-locking; and (iii) high (~100%) yield rate and reliability for manufacturing the device. As presented in Fig. 3.8, successful mode-locking of the fiber ring laser with the VA-SWNT film-based saturable absorber was achieved with the spectral full width at half maximum (FWHM), pulse width and repetition rate of the pulsed output of 2.9 nm, 890 fs and 20.8 MHz, respectively.[35]

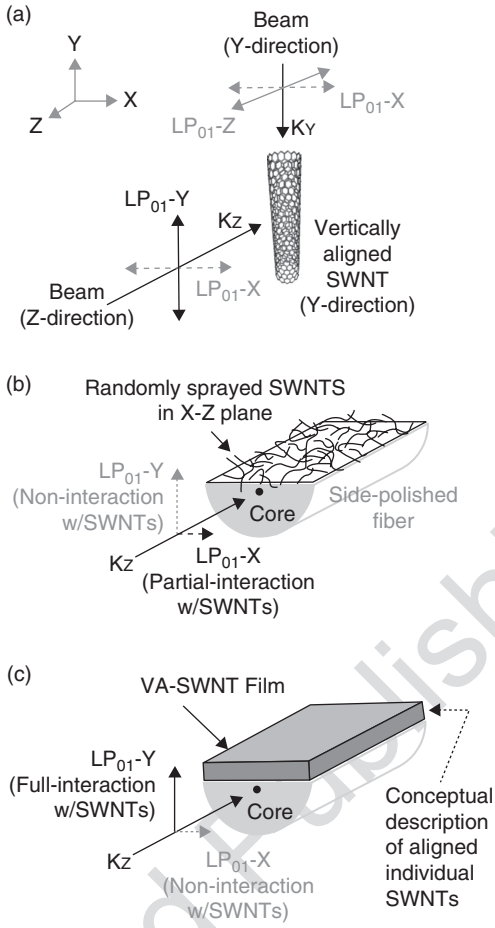

3.6 (a) Schematic explanation of anisotropic optical absorption of an individual SWNT. (b) Conventional operating scheme: partial absorption of the X-polarized mode by randomized SWNTs sprayed on to the X–Z plane. (c) New proposed scheme: maximized absorption of the Y-polarized mode by the vertically aligned SWNT film.

3.3.3 High-energy pulse formation with SWNTs on side-polished fibers

A single stage of high-energy pulse generation without any additional amplification using a SWNT mode locker with a dramatically improved optical damage threshold has been demonstrated.[36] The operation is also based on the evanescent field interaction of propagating light with SWNTs.[30, 35] In the scheme, since only a part of the optical power of the propagating mode interacts with SWNTs to produce mode-locking, higher intracavity power can be introduced

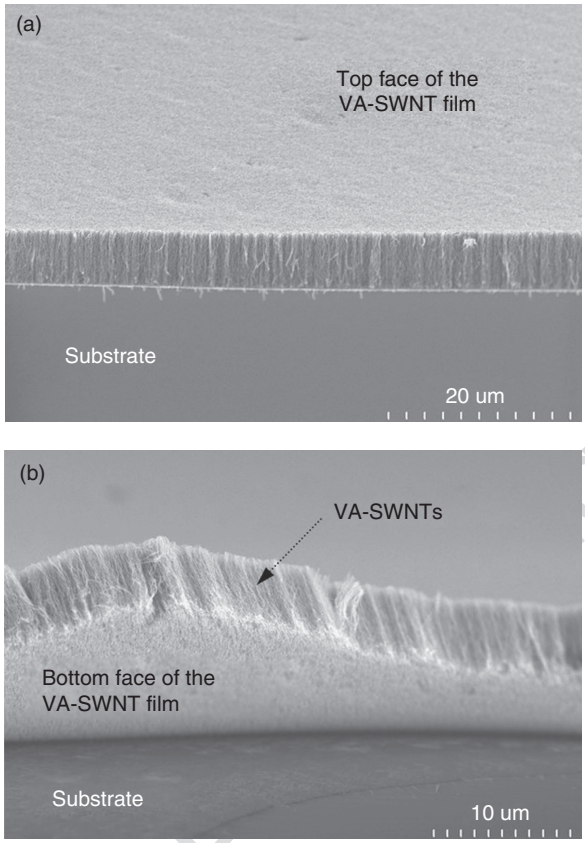

3.7 (a) SEM image of the VA-SWNT film grown on a quartz substrate (×2k). (b) Carpet-like VA-SWNT film peeled away from the substrate (×3k).

for higher energy pulse formation. For both improved operation efficiency and the preparation process, as shown in Fig. 3.9(a), the nanotubes are prepared to form a VA-SWNT, as described in the previous section. The SWNT-substrate interface does not have any significant defect, as Fig. 3.9(b) describes.

The resulting pulsed output has a pulse energy of 6.5 nJ, repetition rate of 38.9 MHz, pulse width of 1.02 ps, and average power of 250 mW (see Fig. 3.10). As illustrated in Fig. 3.11, the output pulses are monitored for over 200 hours to check that there is no significant degradation of the average power or in the output optical spectra.

3.3.4 High-energy pulse formation with graphene

Short laser pulse formation was demonstrated using graphene (reduced graphene oxide to be precise) as a saturable absorber in a high-energy

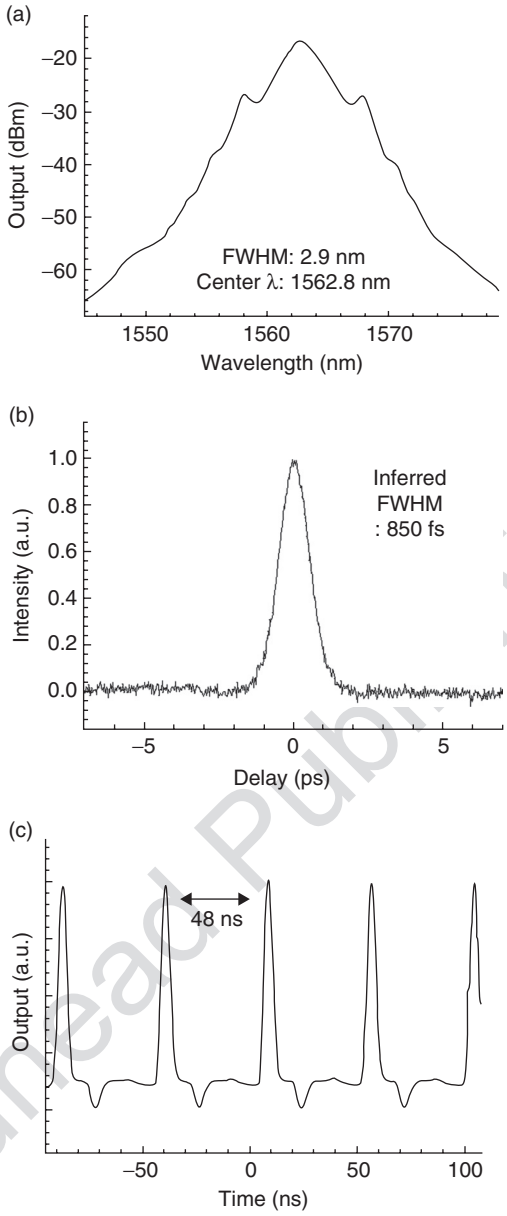

3.8 (a) Output spectrum of our pulsed laser with FWHM of 2.9 nm. (b) Autocorrelation trace of the pulse showing the width of 850 fs. (c) Verification of the pulsed output with pulse train. The repetition rate is 20.8 MHz.

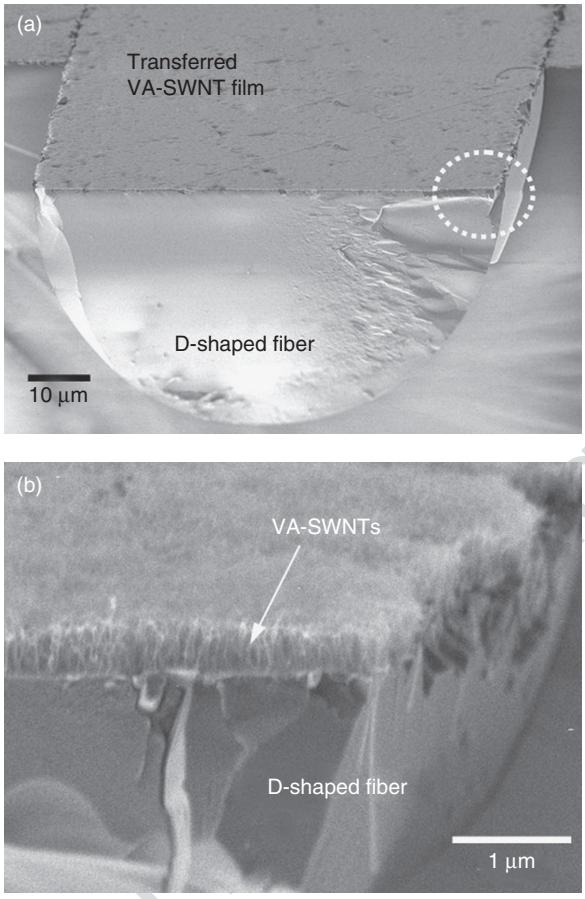

3.9 SEM photos of the SWNT-based all-fiber mode-locking device. (a) Cross-section of the mode locker. The VA-SWNT film is transferred on to the flat surface of the D-shaped fiber. (b) Magnified photo of the encircled area in (a). Individual VA-SWNTs without any significant distortion or defect after the transfer is verified.

management regime.[37,38] To guarantee the safe and robust operation of graphene overcoming optical power-induced thermal damage, an evanescent field interaction scheme of propagating light with graphene deposited on an all-fiber substrate was employed. The mode locker incorporating graphene that was prepared as a graphene suspension and sprayed on to the surface of a side-polished fiber was fabricated as described in Fig. 3.12.

Graphite was chemically oxidized using the modified Hummer method to obtain an aqueous dispersion of graphite oxide, then exfoliation of the graphite oxide under ultrasonication yielded a well-dispersed graphene oxide suspension.[39,40] The graphene oxide in the suspension was reduced

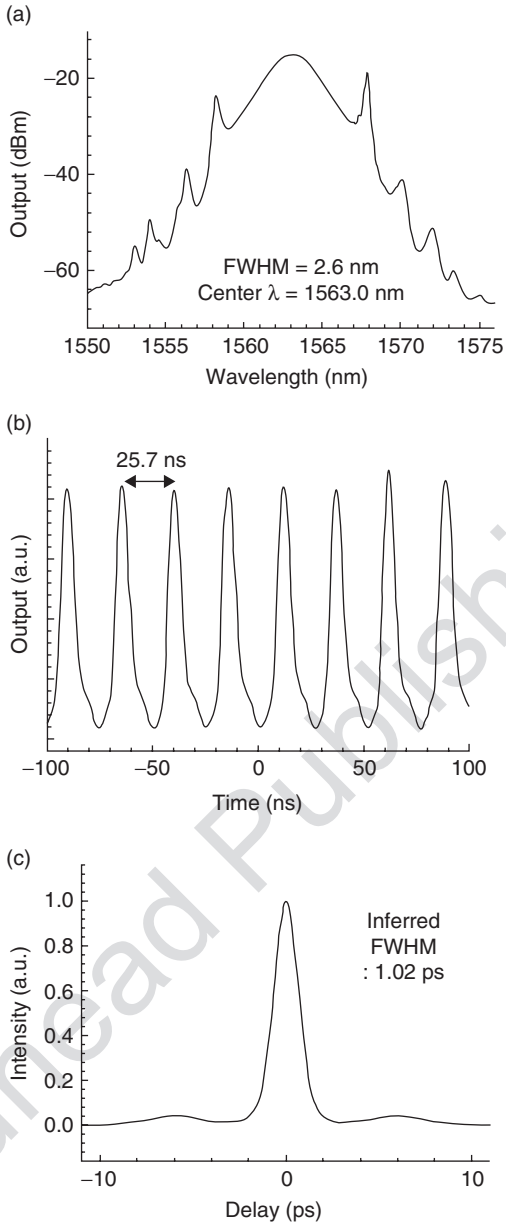

3.10 (a) The optical spectrum of the laser output, and (b) the output pulse train. The spectral FWHM is 2.6 nm, and the repetition rate is 38.9 MHz. (c) Autocorrelation trace of the pulse. The inferred temporal pulse width is 1.02 ps.

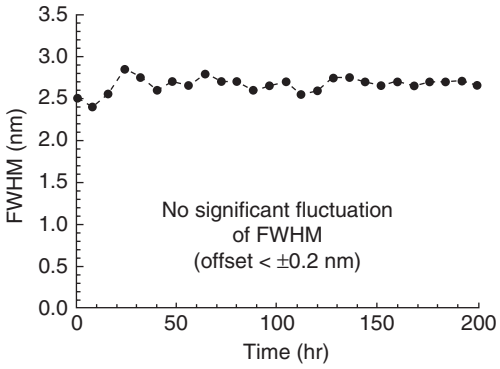

3.11 Long-term operation of the pulsed laser. The fluctuation of the FWHM is negligible. Average power is also not degraded, showing the negligible fluctuation of ±0.03 dBm.

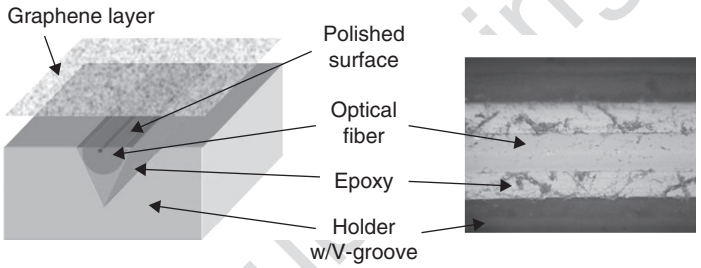

3.12 Prepared fiber mode locker with graphene on a side-polished fiber. (left) Schematic explanation; (right) top-view photo of the polished surface.

using hydrazine hydrate/NH_3 to obtain basic graphene suspension, and then it was neutralized by dialysis. An oil layer was added to the surface of the suspension to prevent oxidation at the air/graphene suspension interface.

The constructed fiber mode-locked laser with graphene is shown in Fig. 3.13, illustrating that the laser has the same structure as the conventional fiber mode-locked laser apart from the graphene-based saturable absorber. The 'lateral interaction scheme' enables graphene to survive with an intracavity optical power higher than 21.4 dBm, guaranteeing safe, nonlinear operation against optical-power-induced thermal damage. It is expected that the lower nonlinear absorption threshold of graphene compared to that of SWNTs increases the efficiency of the pulsation. Moreover, the nonlinear effect of graphene is intensified by employing the evanescent field interaction, in which relatively longer interaction length compared with the direct interaction scheme is applied considering the relation, *Nonlinear*

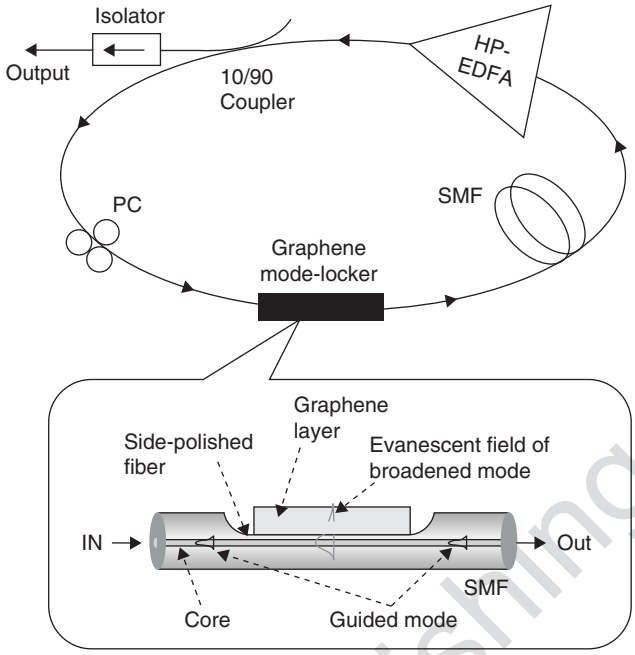

3.13 Fiber mode-locked laser setup. The schematics explain that the guided mode in the fiber core can be broadened by removing the clad so that the evanescent field of the mode can interact with the graphene layer to form the pulses.

$Effect \propto \frac{\gamma PL}{A}$, where γ, P, L, and A are nonlinear coefficient, optical power, interaction length, and interaction area, respectively.

The demonstrated pulse output has center wavelength, spectral width, repetition rate, and estimated pulse duration of 1561.6 nm, 1.96 nm, 6.99 MHz, and 1.3 ps, respectively, as presented in Fig. 3.14.

3.3.5 Single-walled carbon nanotubes coated around tapered fibers

In addition to the side-polished fiber, tapered fiber also has a mode broadening effect, since the volume originally taken by silica can be replaced by air at the tapered waist. Unlike side-polished fibers that have an unavoidable polarization sensitivity, the tapered fibers can provide symmetric mode broadening, thereby ensuring the polarization-immunized operation of the pulse formation. When the device is inserted into a laser cavity, its saturable absorption effect results in pulse formation from the continuous operation of the laser (see Fig. 3.15).[41,42]

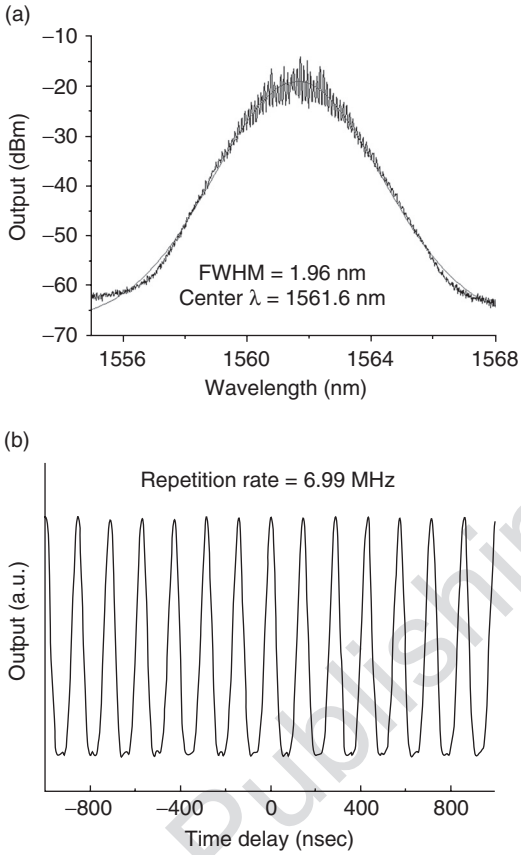

3.14 (a) Optical spectrum; (b) pulse train of the pulse output formed by the graphene mode locker.

The mode broadening in the tapered fiber becomes significant where the diameter of the waist is less than 4 μm, as can be seen in the calculation result, Fig. 3.16(a). Because of the trade-off between the loss induced by the scattering on the surface of the tapered waist and the intensity of the SWNT–light interaction that is proportional to the mode broadening, the waist size should be optimized to create the most effective mode-locking without significant loss from the scattering. Fig. 3.16(b) illustrates the relationships among the waist diameter of the tapered fiber, the scattering loss after the SWNT deposition on to the entire surface of the tapered waist, and the intensity of SWNT–beam interaction. Considering the gain of EDFA in the laser cavity, the loss from the device should be adjusted to less than ~20 dB by controlling the waist diameter and the surface condition of the tapered waist. It was found experimentally that the waist diameter should be reduced to less than ~7 μm to reach the threshold of mode-locking. However, the scattering loss in the

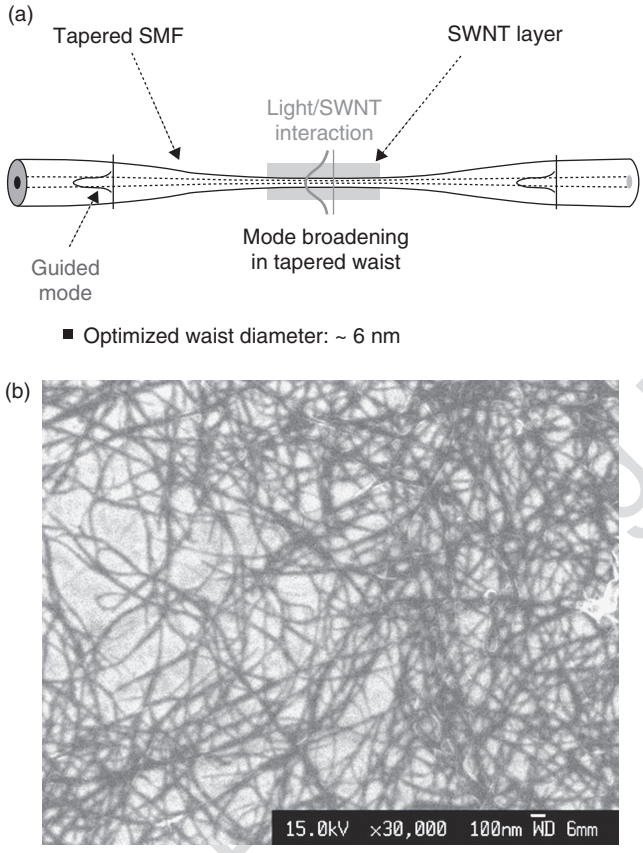

3.15 (a) Conceptual illustration of the pulse formation based on the interaction of SWNTs and the evanescent field of propagating light through a tapered fiber. (b) Morphology of the deposited SWNTs around the 6-μm waist of the tapered fiber (SEM image, x30,000).

case of the 7-μm waist with the complete SWNT coating is measured as much higher than 40 dB. To minimize scattering loss with the thin tapered waist while maintaining the mode-locking operation, SWNTs that act as scattering factors around the limited area of the tapered waist were deposited with the coating length of ~2 mm. Note that while the dispersion change induced in the tapered fiber is significant (from 17 ps/nm.km to 60 ps/nm.km; calculated), the actual dispersion added to the laser cavity is negligible because of the short length of the tapered fiber.

The tapered fiber is prepared by stretching an SMF at an elevated temperature using a coupler machine with a flame size of about 10 mm. The typical length of the tapered region is ~4 cm. The final optimized value of the waist diameter of the tapered fiber is 6 μm, and the insertion loss of the

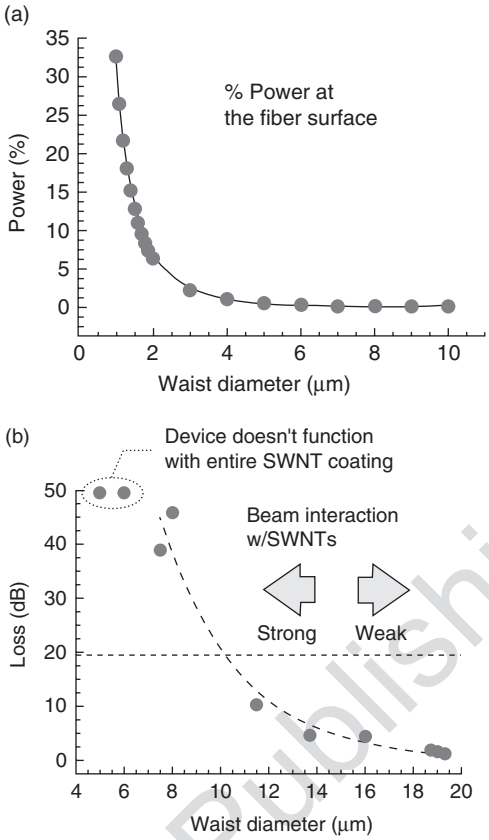

3.16 (a) Calculation result of the mode broadening effect in a tapered fiber. Y-axis indicates the percentage of power detected on the outside of the tapered fiber. (b) The relationship of the waist diameter of the tapered fiber with both the loss and the interaction intensity of the SWNT mode locker where the SWNTs are deposited on to the entire surface of the tapered waist. The fitting line is added on to the measured data points.

device with and without the SWNT coating are 11 dB and <1 dB, respectively. SWNTs are deposited on to the rotating tapered fiber evenly by the spraying method.

The spectrum of the resultant pulsed laser output is shown in Fig. 3.17(a). The center wavelength is 1565 nm. The 3-dB spectral width of 3.1 nm that corresponds to the Δf value of 380 GHz indicates that the temporal FWHM of the output pulse is 829 fs when a transformation-limited sech^2 pulse waveform is assumed. For this output, the pumping current is 400 mA. As shown in Fig. 3.17(b), the pulsed output of our laser is verified by obtaining a pulse train with a repetition rate of 7.3 MHz.

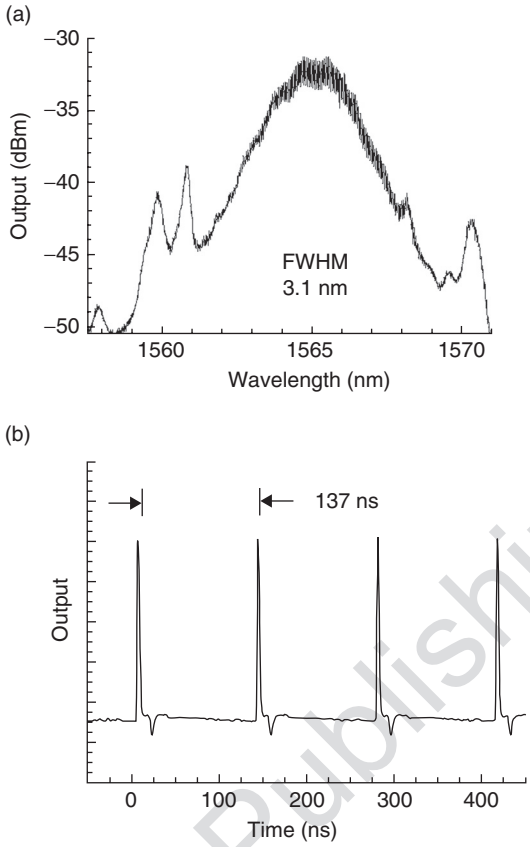

3.17 (a) Optical spectrum of the pulsed laser output measured with the resolution of 0.01 nm; I pump: 400 mA, average power: -9 dBm. (b) Pulse train of our mode-locked laser showing that the pulses are every 137 ns.

3.4 Highly efficient preparation of fiber mode-lockers

One of the important aspects in researching carbon nanostructure-based mode-locked lasers is the improvement in the efficiency of the device-preparation process. Diversified practical processes have been developed intensively in both aspects of the synthesis of carbon nanostructures: in novel approaches as well as in the fabrication of the nanostructure-based mode lockers.

3.4.1 Electrospray of SWNTs

Carbon nanostructures can be deposited on to any photonic components with arbitrary shapes by a simple aerosol spray method after dispersing

individual nanostructures in a highly-dipoled solvent such as DMF. The majority of pulsed lasers rely on a conventional spray process since it is very cost-effective, guaranteeing polarization independence with both homogeneous and randomized deposition of the nanostructures. However, the deposition efficiency of the conventional spray method is very low, to a degree that most SWNTs are lost during the process. Furthermore, large droplet size of the sprayed SWNT suspension can induce agglomeration of the SWNTs. This in turn can lead to deformation of the original morphologies of the individual nanostructures, which are directly correlated with the nonlinear properties of the SWNTs. Thus, it is necessary to explore a deposition method for SWNTs that ensures both high efficiency and reliability of their nonlinear operation.

An electrospray approach for the SWNT spraying was suggested to fabricate the saturable absorption element.[43] Benefits of this method include a target-localized deposition and homogeneous dispersion controlled by the spray geometry as well as nanometer-scaled droplet size. This can be achieved by applying an electrostatic charge on the surface of the original drops on the nozzle tip. The drops are then broken into sub-droplets by electrostatic repulsion overcoming the surface tension of the drop (see Fig. 3.18(a)).[44,45] Fracture of the drops can be encouraged by the potential built between the nozzle and a grounded collecting plate accompanying directional acceleration with a spray angle of about 30°. Compared with conventional sprays, electrospray dramatically improves deposition efficiency with a localized spray within a targeted area while maintaining homogeneity.

As can be seen in Fig. 3.18(b), the current electrospray system consists of a SWNT suspension feeder, a metallic nozzle, a grounded plate, and a high voltage supplier. The sprayed area is determined by the distance (D) between the nozzle tip and the substrate. This distance is minimized to 5 cm to maximize both deposition efficiency and homogeneity. The prepared SWNT suspension is transferred into a feeder and supplied continuously by a syringe pump at a flow rate of 13 μm/min. A high voltage (8 kV) is applied between the nozzle tip and the substrate (distance: 5 cm), resulting in a highly homogeneous and target-localized SWNT deposition on to the flat surface of the side-polished fiber, with an improved deposition efficiency of up to 95% compared with the conventional spray method. Since an electric field cannot be formed on the surface of the side-polished fiber, which has low electric susceptibility, the holding block is covered with aluminum foil apart from the exact area to be sprayed.

Consequently, the fiber mode-locked laser has a pulsed output with a center wavelength, spectral width, and repetition rate of 1559.1 nm, 13.87 nm, and 3.95 MHz, respectively. Because of the ultrafast operation of the device, an estimated pulse duration of 190.9 fs is achieved, as shown in Fig. 3.19.

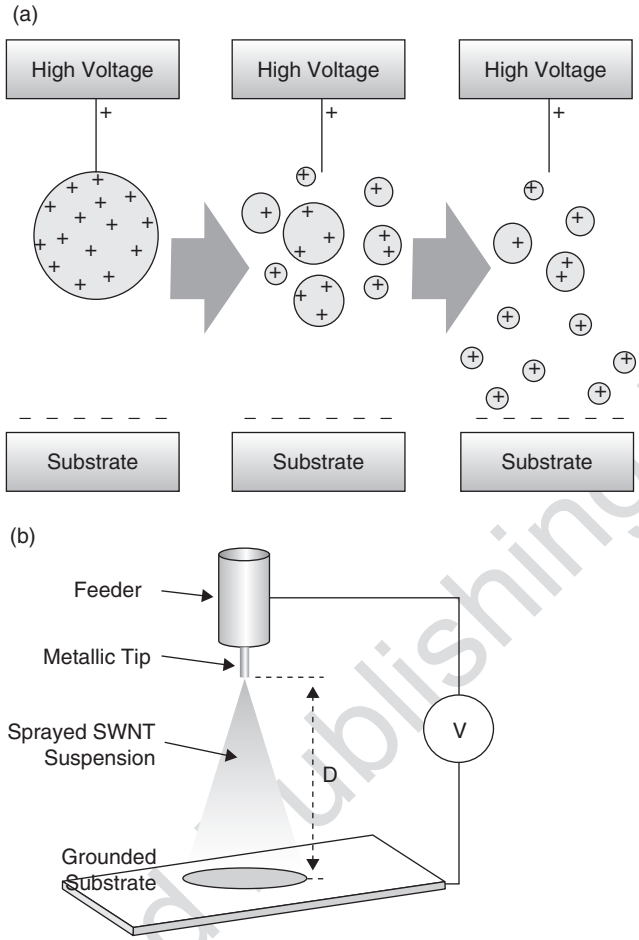

3.18 Schematic explanation of (a) the operation principle, and (b) the experimental setup of the electrospray scheme. In (b), the spray angle is 30°, and D is the nozzle-substrate distance.

3.4.2 Aerosol deposition for SWNT hosting into SiO_2

In spite of the evanescent interaction scheme that allows high-power operation, for more intensified and sophisticated applications of the same carbon nanostructure-based nonlinear elements, it is considered that the direct interaction scheme is still critically attractive, since the nonlinear operation depends mainly on the peak power of the injected light. Unlike the free-standing SWNTs used in direct interaction, the SWNTs in a host material have significant advantages, such as good heat dissipation, high stability, an efficient transfer process to any designed substrate, and good compatibility with other device fabrication processes.[46–48] In particular, a ceramic host

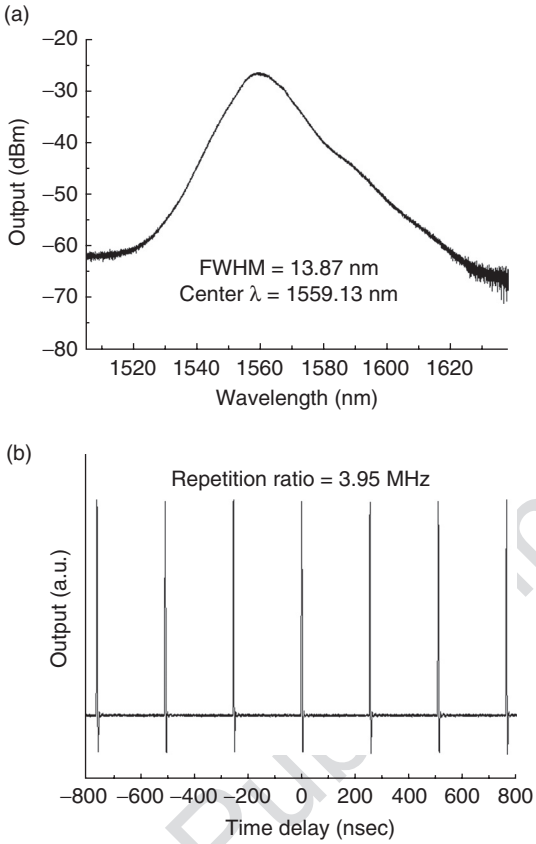

3.19 (a) Optical spectrum of the pulsed laser output, and (b) its pulse train. The spectral width and the repetition rate are 13.87 nm and 3.95 MHz, respectively. The estimated temporal pulse duration is 190.9 fs.

material that can be harmonized with the optical fibers is highly desirable. Moreover, the ceramic host can provide SWNTs with a concrete passivation effect against deleterious oxidation as well as from mechanical attacks.

A room-temperature SiO_2 hosting for SWNTs employing an aerosol deposition (AD) process has been reported.[49–51] The operation principle of AD is based on the shock-loading solidification with the impact of ultrafine ceramic particles on the surface of a substrate. Even with room-temperature and dry deposition conditions, the AD-processed ceramic thick films guarantee the superior densification, with a theoretical density of over 95% for both mechanical toughness and rapid dissipation of the heat generated by the laser-SWNT interaction. The deposition rate of the AD process can reach higher than 1 m/min as a result of its unique deposition mechanism which can be elucidated by the 'crushing and solidification' of submicron-

sized ceramic starting particles.[50] Note that the AD can be free from the solubility limitations of SWNTs that are found in the solution-based sol-gel process and polymer-hosting.

Figure 3.20(a) shows the deposited SiO_2–SWNT composite thick film on the end facet of an optical fiber ferrule. The deposition speed was 2 mm/sec, and the repeat number was 10. The scanning electron microscope (SEM) image shown in Fig. 3.20(b) ensures that a dense microstructure of the SiO_2–SWNT composite thick film can be achieved by AD with the high deposition rate at room temperature. The dispersed SWNTs surrounded by SiO_2 in the composite film can be found in the inset of Fig. 3.20(b). Even though the high impact energy of the starting powders enabled the dense structure by crushing the SiO_2 particles, the morphology of SWNTs were preserved in the film. To confirm the existence of SWNTs, a Raman spectrum of the film deposited on a glass substrate was analyzed. As shown in Fig. 3.21(a), a radial breathing mode (RBM) peak that is an indicating peak corresponding to the coherent vibration of the carbon atoms in the radial direction of the SWNT was detected in the SiO_2–SWNT composite film, and there was negligible peak degradation compared with that of sprayed SWNTs, illustrating that SWNTs in the host still retain their morphological characteristics without significant damage. Figure 3.21(b) shows the transmission curves of the reference SWNTs sprayed on the glass substrate, and the SiO_2–SWNT composite thick film on the glass substrate deposited by the AD. It was verified that the nonlinear absorption level of the hosted SWNTs can be maintained to ~5% in the region of 1550 nm.

One-femtosecond pulses were generated from a single-stage oscillator incorporating the hosted SWNTs, demonstrating the survived carbon nanostructures, and therefore intact nonlinearity under the AD process. Figure 3.22(a) shows the optical spectrum describing the center wavelength and the spectral FWHM are 1599.2 nm and 3.31 nm, respectively. The extinction ratio read in the OSA spectrum was over 30 dB. It can be explained that the noise-like tiny ripples on the spectrum line come from the imperfect connection within the laser cavity, thereby inducing the subcavity effects. Figure 3.22(b) represents the output pulse train formed by the SiO_2-hosted SWNTs, and measured with 10 Gbit/s photo-detector. After suppressing the harmonic mode-locking, we achieved a repetition rate of 9.52 MHz that corresponds to a cavity length of 21.0 m, and illustrates that the formed pulses are from the fundamental mode operation. The temporal pulse duration of the individual pulse was measured by an autocorrelator, as shown in Fig. 3.22(c). The measured FWHM was 890 fs when the data was fitted into the *sech* curve. As the time-frequency product was 0.363, it can be concluded that the generated pulses have a high quality but slightly chirped to approach to the transform-limited pulses. Considering the pulse parameters, the pulse energy and peak power were calculated assuming the

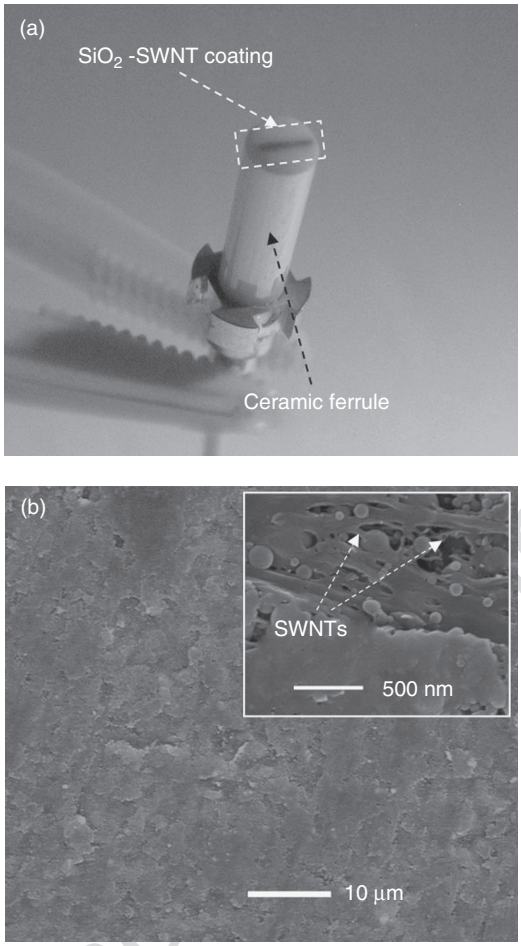

3.20 A SiO_2–SWNT composite film deposited on the end facet of an optical fiber by the AD process: (a) A photograph of the deposited film on the ferrule, and (b) A scanning electron microscope image of the film. A densified ceramic–SWNT composite formed at room temperature can be seen. Inset shows a zoomed-in structure of the composite identifying the SWNT morphologies in the host.

sech pulse formation to be 0.2 nJ and 0.21 kW, respectively, confirming that the fluence level was over the μJ/cm^2 that is typically required for the saturable absorption of SWNTs.[6] The high-power operation of our SiO_2–SWNT sample was also checked with the intracavity power of 20.8 dBm. Unlike the free-standing SWNT that is thermally fragile over the optical power level of 10 dBm in SMF (in case of the direct interaction scheme),[36] the sample still showed the nonlinear intensity modulation after experiencing the high power injection ensuring the critical role of the ceramic hosting.

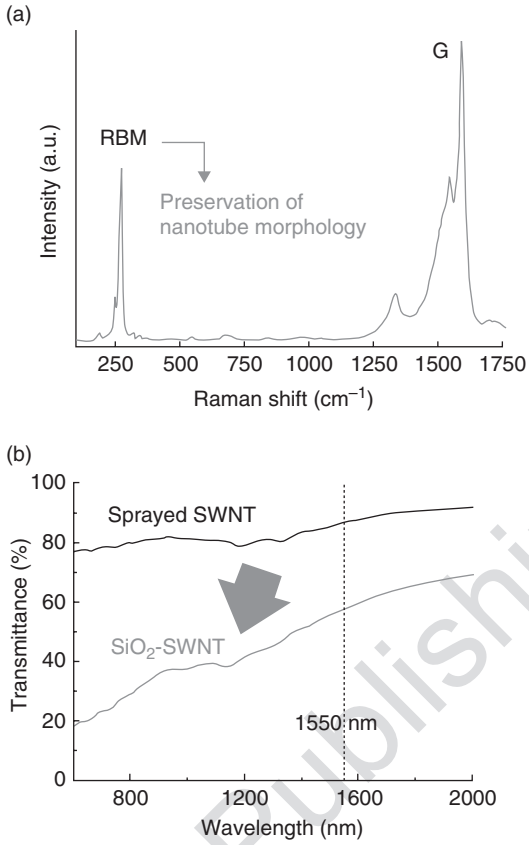

3.21 (a) A Raman spectrum of the deposited SiO_2–SWNT composite film on a glass substrate. A characteristic RBM peak of the SWNT was detected in the film. (b) A transmission curve of the composite film describing the preserved nonlinear absorption peak of SWNTs. The curve was compared with that of the sprayed SWNTs.

3.4.3 Optical deposition of graphene/PVAc

One elegant and simple approach to the deposition of the carbon nanostructures on to the fiber-optic component is the optically driven deposition method that can guarantee efficient, target-focused deposition as well as providing a very simple and safe way to handle the nanostructures.[52] In the case of graphene, distortion and/or deformation during the optical deposition cannot be avoided because of its 2-D morphological characteristics, thereby degrading the nonlinearities that depend greatly on the nano-morphology of graphene.

A circumventing approach was demonstrated, in which the deformation can be suppressed in the optical deposition of graphene by co-dissolving

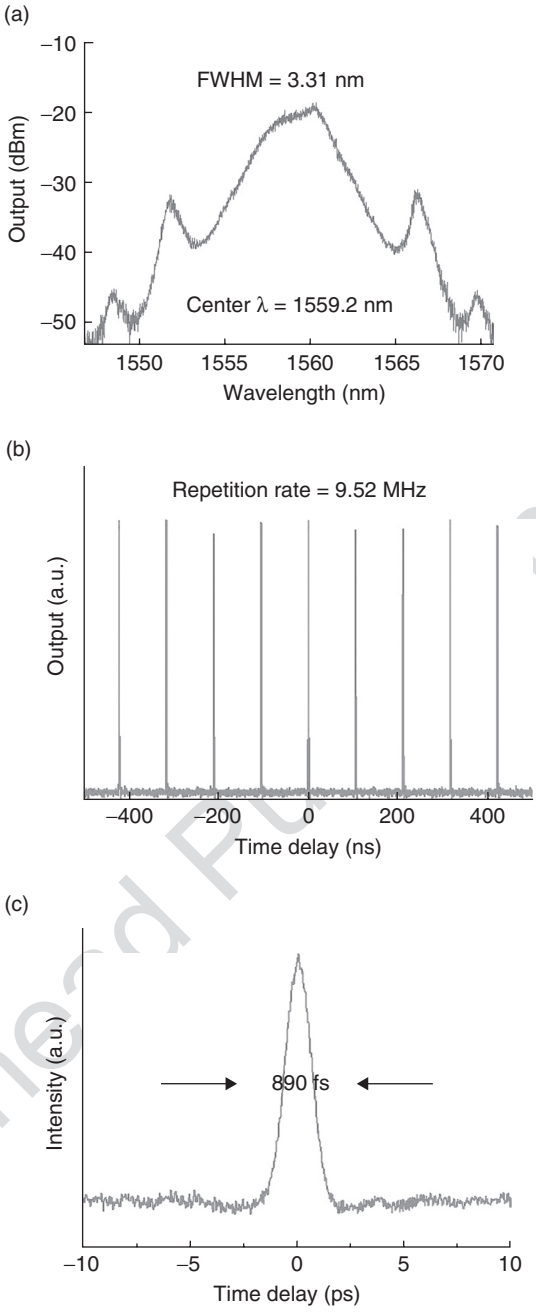

3.22 (a) The measured optical spectrum from the output port. The center wave length and the 3-dB spectral width are 1599.2 nm and 3.31 nm, respectively. (b) The output pulse train measured by the oscilloscope. (c) The autocorrelation trace of an individual output pulse ensuring the successful femtosecond pulse formation.

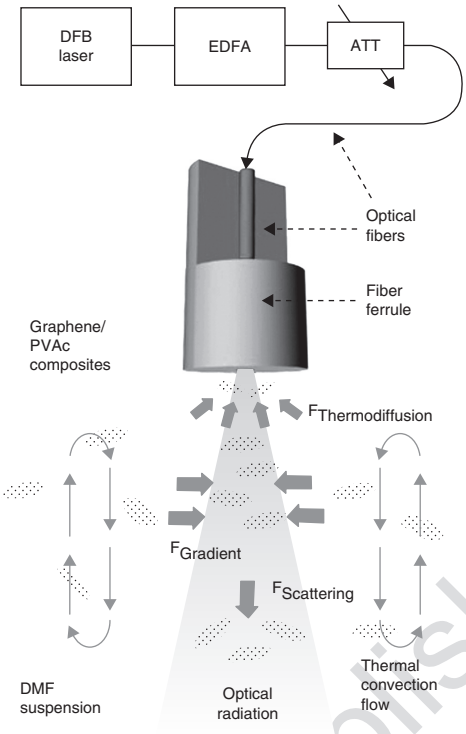

3.23 Conceptual explanation of the optical deposition setup and the deposition mechanisms.

polyvinyl acetate (PVAc) with graphene into dimethylformamide (DMF), therefore PVAc played a critical role during the deposition as a buffer medium to suppress the deformation and/or distortion of graphene.[53] It was determined that the deposition of the graphene/PVAc composite on an optical fiber by laser radiation had three inter-correlated mechanisms, as illustrated in Fig. 3.23, namely (i) optical trapping caused by the interaction of the intensity gradient of the laser beam and the dipole moment of graphene composite; (ii) thermally driven convection flow caused by the local heating of the solution by laser energy;[54] and (iii) thermodiffusion by which nanosheets move along the temperature gradient from the hot liquid suspension heated by the laser to the cold fiber surface.[55] In the optical trapping, two main forces can be considered: scattering force and gradient force, which are proportional to the intensity and the gradient of the laser, respectively.[56] The role of PVAc for graphene deposition was verified by transmission electron microscopy (TEM) and shown in Figs 3.24(a) and 3.24(b), which compare the nano-morphologies of the deposited pure graphene and graphene/PVAc composite, respectively. Unlike pure graphene, the composite

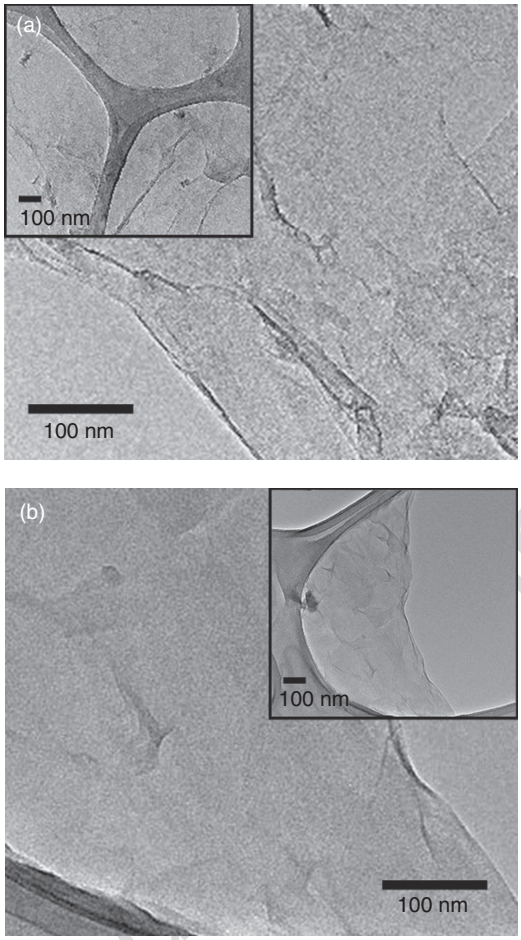

3.24 TEM images of deposited (a) graphene, and (b) graphene/PVAc, with insets of wide-range-view photos.

shows the nanosheet morphology without significant deformation that is critical for the nonlinear properties of graphene. Transmittance characteristics of the deposited composites were also analyzed as shown in Fig. 3.25, ensuring a wide window for the nonlinear operation as well as the crystal-coherence-length dependent light scattering. The inset of Fig. 3.25 illustrates the core-focused deposition of the composites by the optimization of the deposition condition.

Figures 3.26(a) and 3.26(b) are the measured spectra of the deposited pure graphene and graphene/PVAc composite on the fiber core region, respectively. Importantly, the I_D/I_G relative intensity value of the deposited pure graphene ($I_D/I_G = 1.15$) is higher than that of the deposited graphene/PVAc

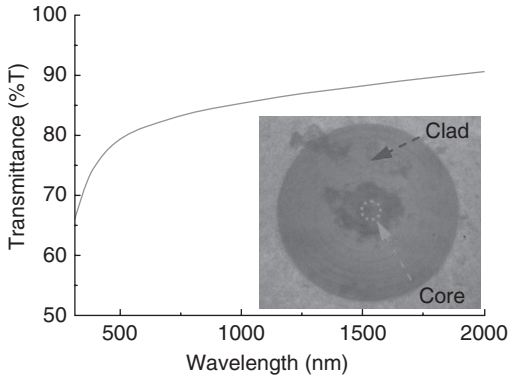

3.25 Transmission characteristics of the graphene/PVAc showing the super-wide operation bandwidth. Inset depicts the core-focused deposition of the graphene composites on to the end facet of an optical fiber.

composite ($I_D/I_G = 0.90$), indicating that the deposited graphene has a higher defect density than the composite. It is analyzed such that the added PVAc provided polymer buffers to graphene, thereby suppressing the deformation of the graphene sheets, and keeping lower defect density by increasing the inter-planar distance between the graphene layers. As a result, the optically deposited graphene/PVAc layer formed the laser pulses passively with the spectral width and repetition rate of 0.6 nm and 91.5 MHz, respectively (see Fig. 3.27).

3.4.4 Mechanically exfoliated graphene

Normally, graphene-saturable absorbers have been made with either a 2D flat graphene thin film attached closely to the end facet of an optical fiber ferrule[19–22] or a sprayed graphene layer on the polished surface of a side-polished fiber for a high-power operating regime[37] providing the successful formation of high-quality femtosecond pulses. Unfortunately, however, the preparation processes of graphene and graphene-based devices still rely on traditional and inefficient approaches, including chemical synthesis tools such as chemical vapor deposition (CVD) and a solution method that cannot be free from the restrictions of additional transfer process steps and the extremely low yield of graphene.[57–59] A dramatically simplified but elegant graphene preparation method based on the mechanical exfoliation of bulk graphite with a strip of adhesive tape was reported very recently.[60, 61] For many years, practical applications of the method have been limited by the size problem of the resulting graphene flakes as well as the difficulty of controlling the monoatomic layer. For its novel application in the research field

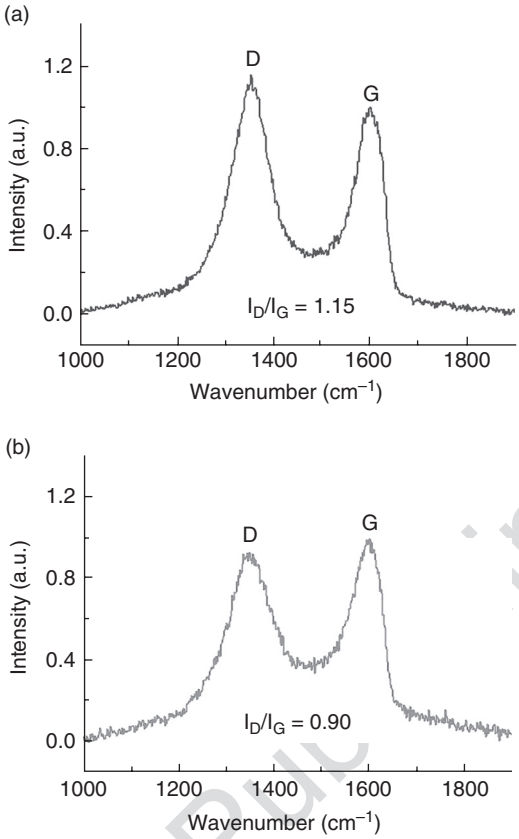

3.26 Raman analysis of (a) pure graphene, and (b) graphene/PVAc composite illustrating that pure graphene has a higher defect density.

of short-pulse laser, a mechanically exfoliated multilayered graphene was prepared and analyzed.[62]

The multilayered graphene on the end facet of the optical fiber ferrule was prepared by the efficient mechanical exfoliation method. The starting material was a highly ordered pyrolytic graphite (HOPG) that was prepared on adhesive tape. Considering the strong interaction between the contact surfaces of the graphite and the optical fiber (amorphous SiO_2) that tended to form a graphite/SiO_2 interface with low interfacial energy, mechanical exfoliation can be applied to the graphene layer formation on the optical fibers.[61,63] After the surface of the optical fiber was cleaned using acetone, ethanol, and deionized water to ensure an uncontaminated surface, the prepared HOPG flakes were pressed with the fiber ferrule according to the sequence described in Fig. 3.28(a)–3.28(c). As a result, thin graphene layers were left on the targeted core area of the optical fiber, as illustrated conceptually in Fig. 3.28(d).

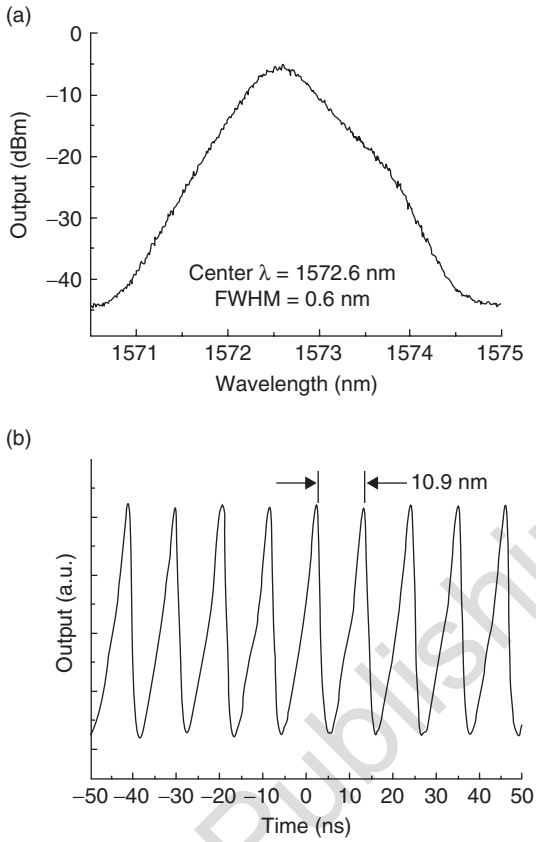

3.27 Pulsed output characteristics of (a) optical spectrum, and (b) pulse train.

The prepared graphene layers were analyzed with atomic force microscopy (AFM). It was found that they had a multilayered morphology with thicknesses ranging from sub-nanometers (2–3 layers) to several nanometers (7–8 layers); see Plate I in the color section between pages 000 and 000. The dimensions of the graphene layer were in the μm scale and thus it can cover the large part of the mode field area of the optical fiber, guaranteeing beam–nanostructure interaction. In Raman analysis, the D peak at 1350 cm $^{-1}$, shown in Fig. 3.29, was correlated to the disorder of the graphene lattice, and the G peak at 1580 cm^{-1} corresponds to the phonon excitation at the Brillouin zone center.[64, 65] The log-scale plot in the figure emphasizes that the D peak has a single and sharp shape as well as low intensity, which represent the high crystal quality of the mechanically exfoliated graphene with no significant defects on it. With a 514-nm excitation, the strong (stronger than the G peak) and narrow shape of the 2D peak at ~2700 cm^{-1} suggests

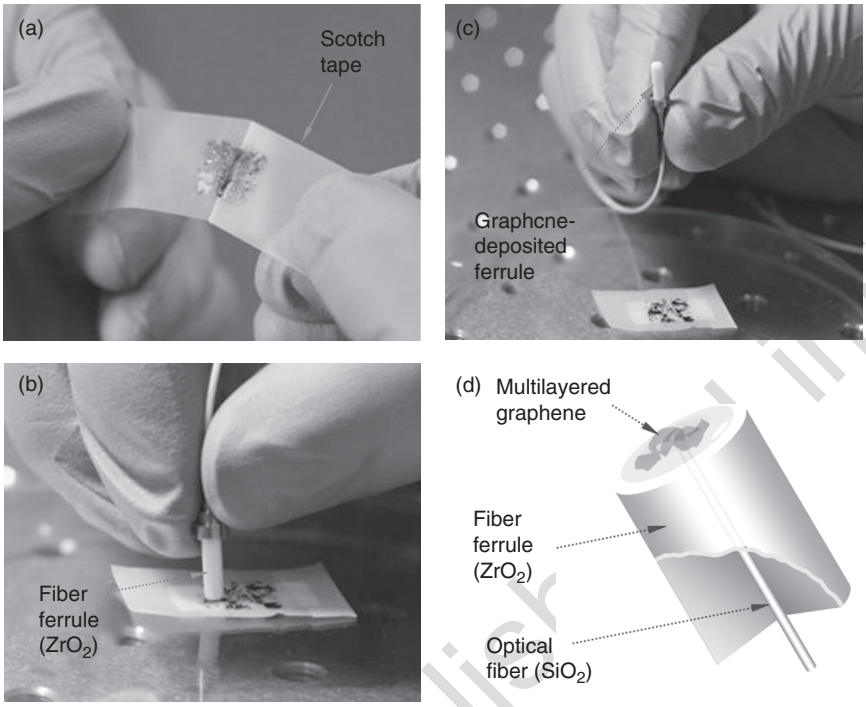

3.28 Graphene preparation on a fiber ferrule. (a) Initial adhesive tape exfoliation of the highly ordered pyrolytic graphite to adjust the thickness. (b) Contact of a surface-cleaned fiber ferrule with the graphite. (c) Careful separation of the ferrule from the graphite. (d) Conceptual explanation of the resultant 'graphene-deposited fiber ferrule'.

that the prepared graphene could have only a few-layered structure. The TEM image shown in the inset of Fig. 3.29 also ensures the few-layered structure of the mechanically prepared graphene.

To apply the adhesive-tape-exfoliated graphene samples to the ultrafast photonic device, a ring cavity of the fiber laser was constructed, as depicted in Fig. 3.30(a). The measured oscilloscope waveform traces of the resultant output pulse trains are shown in Fig. 3.30(b). The pulse period was 91.7 ns, which indicates a repetition rate of 10.9 MHz, which is coincident with the fundamental frequency of the implemented ring cavity, the length of which is estimated to ~19 m. In Fig. 3.30(c), the optical spectra of the mode-locked lasers, measured in a resolution bandwidth of 0.02 nm, are shown together with theoretical sech^2 fitting curves. The 3-dB spectral bandwidth of all the three cases was 0.8 nm. Assuming that the pulses were in transform-limited soliton forms, the estimated output pulse width for the cases was 3.2 ps. The output power of the mode-locked laser was 4.8 dBm irrespective of the

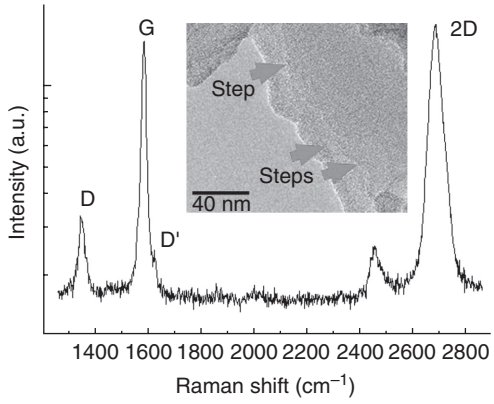

3.29 Raman characterization of the mechanically exfoliated graphene layer in a log scale. Inset shows a TEM image of the terrace-structured graphene.

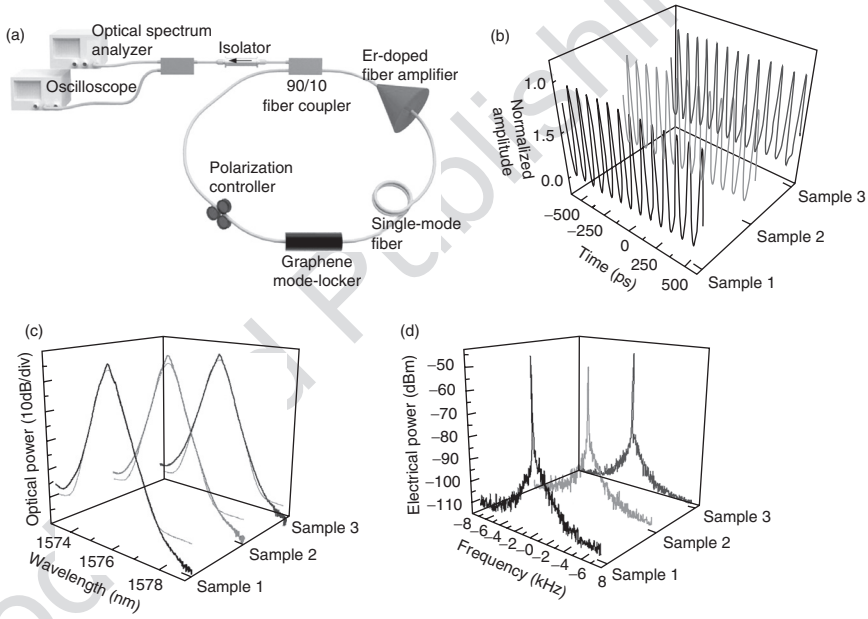

3.30 (a) Experimental setup for a passively pulsed fiber ring laser. (b) Measured oscilloscope waveform traces, (c) optical spectra, and (d) RF spectra of the output pulse trains of samples 1, 2, and 3, which verify the case-insensitive operation of the graphene saturable absorbers that were prepared via mechanical exfoliation.

graphene samples used. The corresponding RF spectra of the output pulses, which were measured under a resolution bandwidth of 300 Hz, are shown in Fig. 3.30(d). The fundamental repetition rate and the peak-to-background ratio were ~10.92 MHz and ~40 dB, respectively, for all three cases, which verifies that the graphene-saturable absorbers used in this work operated successfully as reliable laser pulse formers for future ultrafast photonic devices.

3.5 Conclusion

Since the nonlinear saturable absorption of SWNT was demonstrated initially in 2003,[66] the carbon nanostructure-based mode lockers have been researched extensively in terms of the diversification of spectral/temporal operation ranges, new schemes of light–nanostructure interaction as well as the preparation of nanomaterials and nonlinear devices. Most important, the evanescent field interaction scheme has enabled high-power operation of mode-locked fiber lasers, thereby allowing further research on other nonlinear effects beyond saturable absorption, which is critical to realize highly functional photonic devices. The novel processes, including electrospray, aerosol deposition, optical deposition, and mechanical exfoliation of the carbon nanostructures recorded the remarkably high efficiency of the nonlinear operation and the preparation process. It can be stressed that the research achievements have initiated a new phase of future nonlinear photonics, and can be concrete platforms to realize upgraded carbon nanostructure-functioned novel devices.

3.6 References

1. H. A. Haus, 'Mode-locking of lasers', *IEEE J. Sel. Top. Quant. Electron.*, 2000, **6**, 1173–1185.
2. G. P. Agrawal, '*Nonlinear fiber optics',* Academic Press, 2007, 4th Edition.
3. R. Herda, and O. G. Okhotnikov, 'Dispersion compensation-free fiber laser mode-locked and stabilized by high-contrast saturable absorber mirror', *IEEE J. Quant. Electron.*, 2004, **40**, 893–899.
4. E. U. Rafailov, S. J. White, A. A. Lagatsky, A. Miller, W. Sibbett, D. A. Livshits, A. E. Zhukov, and V. M. Ustinov, 'Fast quantum-dot saturable absorber for passive mode-locking of solid-state lasers', *IEEE Photon Technol. Lett.*, 2004, **16**, 2439–2441.
5. S. Y. Set, H. Yaguchi, Y. Tanaka, and M. Jablonski, 'Laser mode-locking using a saturable absorber incorporating carbon nanotubes', *IEEE J. Lightwave Technol.*, 2004, **22**, 51–56.
6. S. Y. Set, H. Yaguchi, Y. Tanaka, and M. Jablonski, 'Ultrafast fiber pulsed lasers incorporating carbon nanotubes', *IEEE J. Sel. Top. Quant. Electron.*, 2004, **10**, 137–146.
7. S. Iijima, and T. Ichihashi, 'Single-shell carbon nanotubes of 1-nm diameter', *Nature* 1993, **363**, 603–605.

AQ1

8. S. Yamashita, Y. Inoue, S. Maruyama, Y. Murakami, H. Yaguchi, M. Jablonski, and S. Y. Set, 'Saturable absorbers incorporating carbon nanotubes directly synthesized onto substrates/fibers and their applications to mode-locked fiber lasers', *Opt. Lett.*, 2004, **29**, 1581–1583.
9. D. S. Bethune, C. H. Kiang, M. S. DeVries, G. Gorman, R. Savoy, and R. Beyers, 'Cobalt-catalysed growth of carbon nanotubes with single-atomic-layer walls', *Nature* 1993, **363**, 605–607.
10. K. Matsuda, Y. Kanemitsu, K. Irie, T. Saiki, T. Someya, Y. Miyauchi, and S. Maruyama, 'Photoluminescence intermittency in an individual single-walled carbon nanotube at room temperature', *Appl. Phys. Lett.*, 2005, **86**, 123116 (2005).
11. S. Tatsuura, M. Furuki, Y. Sato, I. Iwasa, M. Tian, and H. Mitsu, 'Semiconductor carbon nanotubes a ultrafast switching materials for optical telecommunications', *Adv. Mater.*, 2003, **15**, 534–537.
12. A. K. Geim, and K. S. Novoselov, 'The rise of graphene', *Nature Mater.*, 2007, **6**, 183–191.
13. S. J. Chae, F. Gunes, K. K. Kim, E. S. Kim, G. H. Han, S. M. Kim, H. J. Shin, S. M. Yoon, J. Y. Choi, M. H. Park, C. W. Yang, D. Pribat, and Y. H. Lee, 'Synthesis of large-area graphene layers on poly-nickel substrate by chemical vapor deposition wrinkle formation', *Adv. Mater.*, 2009, **21**, 2328–2333.
14. V. C. Tung, M. J. Allen, Y. Yang, and R. B. Kaner, 'High-throughput solution processing of large-scale graphene', *Nature Nanotech.*, 2009, **4**, 25–29.
15. S. Y. Set, H. Yaguchi, M. Jablonski, Y. Tanaka, Y. Sakakibara, A. Rozhin, M. Tokumoto, H. Kataura, Y. Achiba, and K. Kikuchi, 'A noise suppressing saturable absorber at 1550 nm based on carbon nanotube technology', *Opt. Fiber Comm. Conf. (OFC)*, 2003, FL2.
16. Y. W. Song, S. Y. Set, S. Yamashita, 'Novel Kerr shutter using carbon nanotubes deposited onto a 5-cm D-shaped fiber', *Conf. Laser Electro. Opt. (CLEO)*, 2006, CMA4.
17. K. K. Chow, S. Yamashita, and Y. W. Song, 'A widely tunable wavelength conversion based on nonlinear polarization rotation in a carbon nanotubes deposited D-shaped fiber', *Opt. Exp.*, 2009, **17**, 7664–7669.
18. K. K. Chow and S. Yamashita, 'Four-wave mixing in a single-walled carbon-nanotube-deposited D-shaped fiber and its application in tunable wavelength conversion', *Opt. Exp.*, 2009, **17**, 15608–15613.
19. F. Wang, A. G. Rozhin, V. Scardaci, Z. Sun, F. Hennrich, I. H. White, W. I. Milne, and A. C. Ferrari, 'Wideband-tuneable, nanotube mode-locked, fibre laser', *Nature Nanotech.*, 2008, **3**, 738–742.
20. Q. Bao, H. Zhang, Y. Wang, Z. Ni, Y. Yan, Z. X. Shen, K. P. Loh, and D. Y. Tang, 'Atomic-layer graphene as a saturable absorber for ultrafast pulsed lasers', *Adv. Funct. Mater.*, 2009, **19**, 3077–3083.
21. Z. Sun, T. Hasan, F. Torrisi, D. Popa, G. Privitera, F. Wang, F. Bonaccorso, D. M. Basko, and A. C. Ferrari, 'Graphene mode-locked ultrafast laser', *ACS Nano*, 2010, **4**, 803–810.
22. H. Zhang, Q. Bao, D. Tang, L. Zhao, and K. Loh, 'Large energy soliton erbium-doped fiber laser with a graphene-polymer composite mode locker', *Appl. Phys. Lett.*, 2009, **95**, 141103–1–3.
23. A. H. Castro Neto, F. Guinea, N. M. R. Peres, K. S. Novoselov, and A. K. Geim, 'The electronic properties of graphene', *Rev. Mod. Phys.*, 2009, **81**, 109–162.

24. G. Xing, H. Guo, X. Zhang, T. C. Sum, and C. H. A. Huan, 'The physics of ultrafast saturable absorption in graphene', *Opt. Exp.* 2010, **18**, 4564–4573.
25. R. W. Newson, J. Dean, B. Schmidt, and H. M. van Driel, 'Ultrafast carrier kinetics in exfoliated graphene and thin graphite films', *Opt. Exp.*, 2009, **17**, 2326–2333.
26. P. L. McEuen, M. S. Fuhrer, and H. K. Park, 'Single-walled carbon nanotube electronics', *IEEE Trans Nanotech.*, 2002, **1**, 78–85.
27. D. Li, M. B. Müller, S. Gilje, R. B. Kaner, and G. G. Wallace, 'Processable aqueous dispersions of graphene nanosheets, ' *Nature Nanotech.*, 2008, **3**, 101–105.
28. R. R. Nair, P. Blake, A. N. Grigorenko, K. S. Novoselov, T. J. Booth, T. Stauber, N. M. R. Peres, and A. K. Geim, 'Fine structure constant defines visual transparency of graphene', *Science*, 2008, **320**, 1308.
29. S. Yamashita, Y. Inoue, S. Maruyama, Y. Murakami, H. Yaguchi, M. Jablonski, and S. Set, 'Saturable absorbers incorporating carbon nanotubes directly synthesized onto substrates and fibers and their application to mode-locked fiber lasers', *Opt. Lett.*, 2004, **29**, 1581–1583.
30. Y. W. Song, S. Yamashita, C. S. Goh, and S. Y. Set, 'Carbon nanotube mode-lockers with enhanced nonlinearity via evanescent field interaction in D-shaped fibers', *Opt. Lett.*, 2007, **32**, 148–150.
31. Y. Murakami, E. Einarsson, T. Edamura, and S. Maruyama, 'Polarization dependence of the optical absorption of single-walled carbon nanotubes', *Phys. Rev. Lett.*, 2005, **94**, 087402–1–4.
32. B. W. Reed, and M. Sarikaya, 'Electronic properties of carbon nanotubes by transmission electron energy-loss spectroscopy', *Phys. Rev. B*, 2001, **64**, 195404–1–13.
33. Y. Murakami, E. Einarsson, T. Edamura, and S. Maruyama, 'Polarization dependent optical absorption properties of single-walled carbon nanotubes and methodology for the evaluation of their morphology', *Carbon* 2005, **43**, 2664–2676.
34. Y. Murakami, S. Chiashi, Y. Miyauchi, M. Hu, M. Ogura, T. Okubo, and S. Maruyama, 'Growth of vertically aligned single-walled carbon nanotube films on quartz substrates and their optical anisotropy', *Chem. Phys. Lett.*, 2004, **385**, 298–303.
35. Y. W. Song, S. Yamashita, E. Einarsson, and S. Maruyama, 'All-fiber pulsed lasers passively mode-locked by transferable vertically aligned carbon nanotube film', *Opt. Lett.*, 2007, **32**, 1399–1401.
36. Y. W. Song, S. Yamashita, and S. Maruyama, 'Single-walled carbon nanotubes for high-energy optical pulse formation', *Appl. Phys. Lett.*, 2008, **92**, 021115–1–3.
37. Y. W. Song, S. Y. Chang, W. S. Han, and M. K. Bae, 'A graphene mode-locker for fiber lasers passively pulsed by evanescent field interaction', *Appl. Phys. Lett.*, 2010, **96**, 051122–1–3.
38. Nature Photonics Research Highlights, 'Graphene: under high energy', *Nature Photon.*, 2010, **4**, 196.
39. W. S. Hummers, and R. E. Offeman, 'Preparation of Graphitic Oxide', *J. Am. Chem. Soc.*, 1958, **80**, 1339–1339.
40. S. Stankovich, D. A. Dikin, R. D. Piner, K. A. Kohlhaas, A. Kleinhammes, Y. Jia, Y. Wu, S. T. Nguyen, and R. S. Ruoff, 'Synthesis of graphene-based nanosheets via chemical reduction of exfoliated graphite oxide', *Carbon* 2007, **45**, 1558–1565.

41. Y. W. Song, K. Morimune, S. Y. Set, and S. Yamashita, 'Polarization insensitive all-fiber mode-lockers functioned by carbon nanotubes deposited onto tapered fibers', *App. Phys. Lett.*, 2007, **90**, 021101–1–3.
42. K. Kieu and M. Mansuripur, 'Femtosecond laser pulse generation with a fiber taper embedded in carbon nanotube/polymer composite', *Opt. Lett.*, 2007, **32**, 2242–2244.
43. S. H. Chu, W. S. Han, I. D. Kim, Y. G. Han, K. I. Lee, S. B. Lee, and Y. W. Song, 'Ultrafast saturable absorption devices incorporating efficiently electrosprayed carbon nanotubes', *Appl. Phys. Lett.*, 2010, **96**, 051111–1–3.
44. J. S. Suh, B. W. Han, K. Okuyama, and M. S. Choi, 'Highly charging of nanoparticles through electrospray of nanoparticle suspension', *J. colloid interface sci.*, 2005, **287**, 135–140.
45. A.M. Gañan-Calvo, J. Davila, and A. Barrero, 'Current and droplet size in the electrospraying of liquids. Scaling laws', *J. Aerosol Sci.*, 1997, **28**, 249–275.
46. Z. Xia, L. Riester, W.A. Curtin, H. Li, B.W. Sheldon, J. Liang, B. Chang, and J.M. Xu, 'Direct observation of toughening mechanisms in carbon nanotube ceramic matrix composites', *Acta Mater.*, 2004, **52**, 931–944.
47. R. Andrews and M.C. Weisenberger, 'Carbon nanotube polymer composites', *Curr. Opin. Solid State Mat. Sci.*, 2004, **8**, 31–37.
48. H. G. Chae, M. L. Minus, A. Rasheed, and S. Kumar, 'Stabilization and carbonization of gel spun polyacrylonitrile/single wall carbon nanotube composite fibers', *Polymer*, 2007, **48**, 3781–3789.
49. H. J. Kim, H. J. Choi, S. M. Nam, and Y. W. Song, 'High-performance laser mode-locker with glass-hosted SWNTs realized by room-temperature aerosol deposition', *Opt. Exp.*, 2011, **19**, 4762–4767.
50. J. Akedo, 'Room temperature impact consolidation (RTIC) of fine ceramic powder by aerosol deposition method and applications to microdevices', *J. Therm. Spray Techn.*, 2008, **17**, 181–198.
51. S. M. Nam, N. Mori, H. Kakemoto, S. Wada, J. Akedo and T. Tsurumi, 'Alumina thick films as integral substrates using aerosol deposition method', *Jpn. J. Appl. Phys.*, 2004, **43**, 5414–5418.
52. J. W. Nicholson, R. S. Windeler, and D. J. DiGiovanni, 'Optically driven deposition of single-walled carbon-nanotube saturable absorbers on optical fiber end-faces', *Opt. Exp.*, 2007, **15**, 9176–9183.
53. H. S. Kim, J. H. Cho, S. Y. Chang, and Y. W. Song, 'Deformation-immunized optical deposition of graphene for ultrafast pulsed lasers', *Appl. Phys. Lett.*, 2011, **98**, 021104–1–3.
54. P. W. Smith, A. Ashkin, and W. J. Tomlinson, 'Four-wave mixing in an artificial Kerr medium', *Opt. Lett.*, 1981, **6**, 284–286.
55. G. S. McNab, and A. Meisen, 'Thermophoresis in liquids', *J. Colloid Interface Sci.*, 1973, **44**, 339–346.
56. A. Ashkin, J. M. Dziedzic, J. E. Bjorkholm, and C. Steven, 'Observation of a single-beam gradient force optical trap for dielectric particles, ' *Opt. Lett.*, 1986, **11**, 288–290.
57. A. Reina, X. Jia, J. Ho, D. Nezich, H. Son, V. Bulovic, M. S. Dresselhaus, and J. Kong, 'Large Area, few-layer graphene films on arbitrary substrates by chemical vapor deposition', *Nano Lett.*, 2009, **9**, 30–35.
58. Y. Si, and E. T. Samulski, 'Synthesis of water soluble graphene', *Nano Lett.*, 2008, **8**, 1679–1682.

59. S. Pang, H. N. Tsao, S. Feng, and K. Mullen, 'Patterned Graphene Electrodes from Solution-Processed Graphite Oxide Films for Organic Field-Effect Transistors', *Adv. Mater.*, 2009, **21**, 3488–3491.
60. S. Wang, P. K. Ang, Z. Wang, A. L. L. Tang, J. T. L. Thong, and K. P. Loh, 'High Mobility, Printable, and Solution-Processed Graphene Electronics', *Nano Lett.*, 2010, **10**, 92–98.
61. M. Hulman, M. Haluska, G. Scalia, D. Obergfell, and S. Roth, 'Effect of charge impurities and laser energy on Raman spectra of graphene', *Nano Lett.*, 2008, **8**, 3594–3597.
62. Y. M. Chang, H. S. Kim, J. H. Lee, and Y. W. Song, 'Multilayered graphene efficiently formed by mechanical exfoliation for ultrafast photonics', *Appl. Phys. Lett.*, 2010, **97**, 211102–1–3.
63. D. Li, W. Windl, and N. P. Padture, 'Toward site-specific stamping of graphene', *Adv. Mater.*, 2009, **21**, 1243–1246.
64. C. Casiraghi, A. Hartschuh, H. Qian, S. Piscanec, C. Georgi, A. Fasoli, K. S. Novoselov, D. M. Basko, and A. C. Ferrari, 'Raman Spectroscopy of Graphene Edges', *Nano Lett.*, 2009, **9**, 1433–1441.
65. Z. H. Ni, H. M. Wang, J. Kasim, H. M. Fan, T. Yu, Y. H. Wu, Y. P. Feng, and Z. X. Shen, 'Graphene Thickness Determination Using Reflection and Contrast Spectroscopy', *Nano Lett.*, 2007, **7**, 2758–2763.
66. S. Y. Set, H. Yaguchi, Y. Tanaka, M. Jablonski, Y. Sakakibara, A. Rozhin, M. Tokumoto, H. Kataura, Y. Achiba, and K. Kikuchi, 'Mode-locked fiber lasers based on a saturable absorber incorporating carbon nanotubes', *Opt. Fiber Comm. Conf. (OFC)*, 2003, PD44.

AQ1 Please provide place of publication for the reference.